

# Defective Fluid Secretion and NaCl Absorption in the Parotid Glands of $\text{Na}^+/\text{H}^+$ Exchanger-deficient Mice\*

Received for publication, April 2, 2001, and in revised form, May 17, 2001  
Published, JBC Papers in Press, May 17, 2001, DOI 10.1074/jbc.M102901200

Keerang Park<sup>‡\$¶</sup>, Richard L. Evans<sup>‡\$¶</sup>, Gene E. Watson<sup>\$¶</sup>, Keith Nehrke<sup>‡\$¶</sup>, Linda Richardson<sup>‡</sup>, Sheila M. Bell<sup>\*\*</sup>, Patrick J. Schultheis<sup>‡‡</sup>, Arthur R. Hand<sup>§§</sup>, Gary E. Shull<sup>‡‡</sup>, and James E. Melvin<sup>‡\$¶</sup>

From the <sup>‡</sup>Center for Oral Biology, Rochester Institute of Biomedical Sciences, and the <sup>\$</sup>Eastman Department of Dentistry, University of Rochester Medical Center, Rochester, New York 14642, the <sup>§§</sup>Department of Pediatric Dentistry, University of Connecticut, Farmington, Connecticut 06030, the <sup>‡‡</sup>Department of Molecular Genetics, Biochemistry and Microbiology, University of Cincinnati College of Medicine, Cincinnati, Ohio 45267, and the <sup>\*\*</sup>Division of Developmental Biology, Children's Hospital Research Foundation, Cincinnati, Ohio 45229

**Multiple  $\text{Na}^+/\text{H}^+$  exchangers (NHEs) are expressed in salivary gland cells; however, their functions in the secretion of saliva by acinar cells and the subsequent modification of the ionic composition of this fluid by the ducts are unclear. Mice with targeted disruptions of the *Nhe1*, *Nhe2*, and *Nhe3* genes were used to study the *in vivo* functions of these exchangers in parotid glands. Immunohistochemistry indicated that NHE1 was localized to the basolateral and NHE2 to apical membranes of both acinar and duct cells, whereas NHE3 was restricted to the apical region of duct cells.  $\text{Na}^+/\text{H}^+$  exchange was reduced more than 95% in acinar cells and greater than 80% in duct cells of NHE1-deficient mice (*Nhe1*<sup>-/-</sup>). Salivation in response to pilocarpine stimulation was reduced significantly in both *Nhe1*<sup>-/-</sup> and *Nhe2*<sup>-/-</sup> mice, particularly during prolonged stimulation, whereas the loss of NHE3 had no effect on secretion. Expression of  $\text{Na}^+/\text{K}^+/2\text{Cl}^-$  cotransporter mRNA increased dramatically in *Nhe1*<sup>-/-</sup> parotid glands but not in those of *Nhe2*<sup>-/-</sup> or *Nhe3*<sup>-/-</sup> mice, suggesting that compensation occurs for the loss of NHE1. The sodium content, chloride activity and osmolality of saliva in *Nhe2*<sup>-/-</sup> or *Nhe3*<sup>-/-</sup> mice were comparable with those of wild-type mice. In contrast, *Nhe1*<sup>-/-</sup> mice displayed impaired NaCl absorption. These results suggest that in parotid duct cells apical NHE2 and NHE3 do not play a major role in  $\text{Na}^+$  absorption. These results also demonstrate that basolateral NHE1 and apical NHE2 modulate saliva secretion *in vivo*, especially during sustained stimulation when secretion depends less on  $\text{Na}^+/\text{K}^+/2\text{Cl}^-$  cotransporter activity.**

Saliva formation is thought to involve a two-stage process (1–3). Initially, acinar cells secrete an isotonic plasma-like fluid, the generation of which depends on the coordinated ac-

tivity of a number of membrane transport proteins that drive net transepithelial  $\text{Cl}^-$  movement and significant  $\text{HCO}_3^-$  efflux (see Refs. 4 and 5). The available evidence suggests that  $\text{Cl}^-$  uptake across the basolateral membrane of acinar cells is primarily mediated via the electroneutral  $\text{Na}^+/\text{K}^+/2\text{Cl}^-$  cotransporter. This has been demonstrated clearly in mice lacking expression of the *Nkcc1*<sup>1</sup> gene, in which pilocarpine-stimulated secretion is greatly reduced but not eliminated (6). *In situ*, the main fluid and electrolyte agonist acetylcholine triggers secretion by increasing the  $\text{Cl}^-$  and  $\text{HCO}_3^-$  permeability of the apical membrane.  $\text{HCO}_3^-$  efflux via the apical anion channel produces an intracellular acid load that is rapidly buffered by an increase in  $\text{Na}^+/\text{H}^+$  exchanger activity (7–9). Therefore, the residual secretion from NKCC1-deficient mice is likely mediated by enhanced  $\text{Na}^+/\text{H}^+$  exchange, which drives  $\text{Cl}^-$  uptake via the coupled operation of  $\text{Na}^+/\text{H}^+$  and  $\text{Cl}^-/\text{HCO}_3^-$  exchangers as well as carbonic anhydrase- and  $\text{Na}^+/\text{H}^+$  exchanger-dependent  $\text{HCO}_3^-$  efflux (5).

During the second stage of secretion, ductal cells modify acinar secretions primarily by conserving NaCl in a flow rate-dependent fashion; and because the apical surfaces of salivary ducts are relatively impermeant to water, saliva is generally hypotonic (see Refs. 4 and 5). A “typical” NaCl-conserving duct cell is thought to possess at least two  $\text{Na}^+$  uptake mechanisms. The first of these is  $\text{Na}^+/\text{H}^+$  exchange located in the luminal membrane (10–12). Of the different  $\text{Na}^+/\text{H}^+$  exchanger (NHE) isoforms expressed in salivary gland duct cells, NHE2 and NHE3 are thought to be associated with  $\text{Na}^+$  absorption in other epithelial tissues (see Refs. 13 and 14). A second mechanism for  $\text{Na}^+$  uptake by salivary gland duct cells is an amiloride-sensitive  $\text{Na}^+$  channel (15). This channel has properties comparable with the cloned epithelial  $\text{Na}^+$  channel ENaC (16), which is involved in  $\text{Na}^+$  absorption in the kidney and lungs (see Ref. 17).

Consistent with the two-stage secretion model, inhibitor studies suggest that  $\text{Na}^+/\text{H}^+$  exchangers may contribute both to fluid and electrolyte secretion from acinar cells and to reabsorption of NaCl by duct cells (18–22). The relative lack of specificity of these inhibitors makes it unclear as to which NHE isoforms are involved. The mammalian NHE gene family consists of six isoforms (13, 14). Of these, NHE1, NHE2, NHE3, and NHE4 are expressed in the plasma membrane of epithelial

\* This work was supported in part by National Institutes of Health Grants DK50594 (to G. E. S.), DE08921, and DE09692 (to J. E. M.). The costs of publication of this article were defrayed in part by the payment of page charges. This article must therefore be hereby marked “advertisement” in accordance with 18 U.S.C. Section 1734 solely to indicate this fact.

¶ These authors contributed equally to this study.

\*\* Present address: Unilever Research, Port Sunlight Laboratory, Quarry Rd. East, Bebington, Wirral CH63 3JW, United Kingdom. E-mail: Richard.Evans@Unilever.com.

† To whom correspondence should be addressed: Center for Oral Biology, Univ. of Rochester, Medical Center Box 611, 601 Elmwood Ave., Rochester, NY 14642. Tel.: 716-275-3444; Fax: 716-473-2679; E-mail: james\_melvin@urmc.rochester.edu.

<sup>1</sup> The abbreviations used are: NKCC1,  $\text{Na}^+/\text{K}^+/2\text{Cl}^-$  cotransporter isoform 1; NHE1–NHE4,  $\text{Na}^+/\text{H}^+$  exchanger isoforms 1–4; ENaC, epithelial  $\text{Na}^+$  channel;  $\alpha$ ,  $\beta$ , and  $\gamma$ -ENaC,  $\alpha$ ,  $\beta$ , and  $\gamma$  subunits of ENaC; nts, nucleotides.

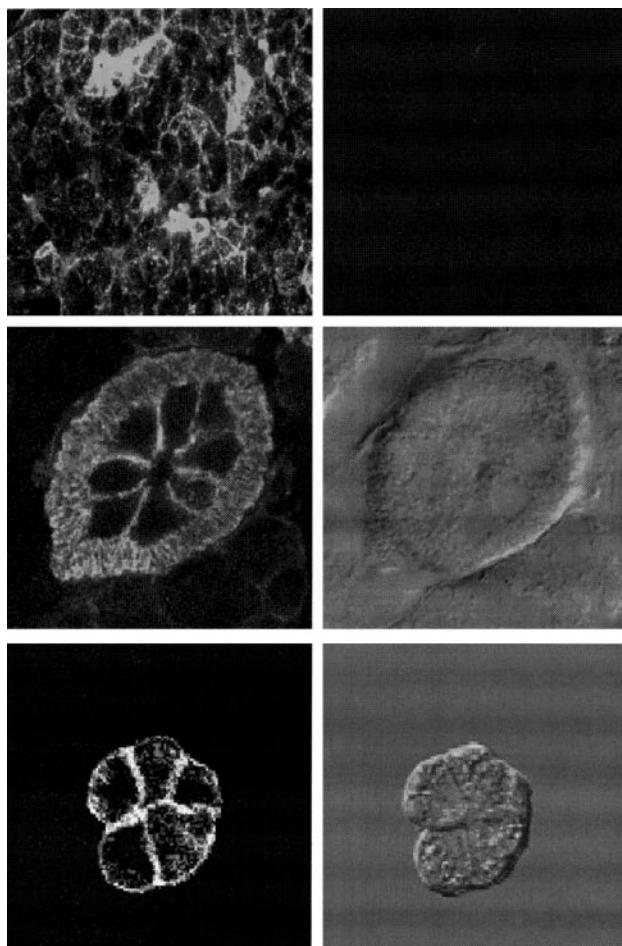


**FIG. 1. Immunolocalization of NHE1 to the basolateral membrane of acinar and ductal cells in mouse parotid gland.** Paraffin-embedded sections or isolated cells from wild-type (+/+) and *Nhe1* null mutant (−/−) animals were treated as described under “Experimental Procedures,” incubated overnight with polyclonal anti-NHE1 antibody, and then treated with fluorescent-labeled secondary antibody. *Top left panel*, a section from wild-type parotid gland treated with the anti-NHE1 antibody shows specific staining of the basolateral membrane of acinar cells. *Top right panel*, the anti-NHE1 antibody shows no specific staining in a parotid section prepared from *Nhe1* null mutant animals. *Middle left panel*, a section from wild-type parotid gland treated with the anti-NHE1 antibody shows intense specific staining of the basolateral membrane of a duct cut in cross-section. *Middle right panel*, a Nomarski image of the same duct shown in the *middle left panel*. *Bottom left panel*, an enzymatically isolated acinus from wild-type parotid gland treated with anti-NHE1 antibody shows specific staining of the basolateral membrane. *Bottom right panel*, a Nomarski image of the same acinus shown in the *bottom left panel*.

tissues including salivary glands (10–12, 23). However, little is known about the specific functions of the individual NHE isoforms in salivary glands. To determine the molecular identity of the  $\text{Na}^+/\text{H}^+$  exchangers involved in the above processes, we examined the effects of *Nhe1*, *Nhe2*, and *Nhe3* gene disruptions on mouse parotid gland function. Our results demonstrate that  $\text{Na}^+/\text{H}^+$  exchanger isoforms NHE1 and NHE2, which are located in the basolateral and apical membranes of acinar cells, respectively, are important regulators of saliva secretion *in vivo*. Furthermore, the loss of NHE2 or NHE3 does not inhibit NaCl absorption by duct cells, whereas NaCl absorption was blunted in NHE1-deficient mice. Unexpectedly, these results suggest that neither NHE2 nor NHE3 are primary  $\text{Na}^+$  absorption mechanisms in mouse parotid glands.

#### EXPERIMENTAL PROCEDURES

**Materials and Null Mutant Animals**—All chemicals were from Sigma. Targeted disruptions of the murine *Nhe1*, *Nhe2*, and *Nhe3* genes

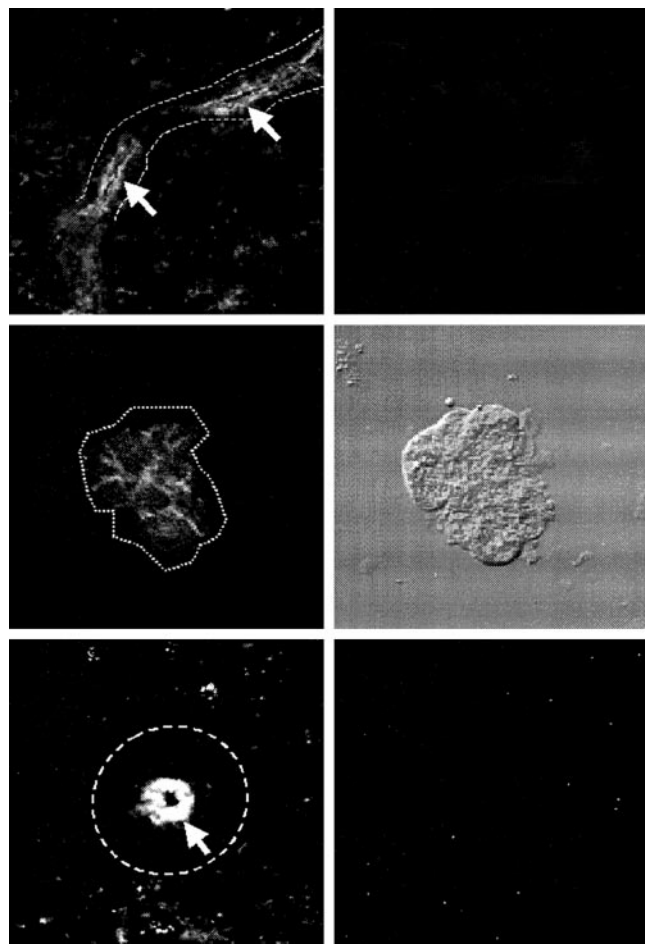


**FIG. 2. Immunolocalization of NHE2 and NHE3 in mouse parotid gland.** Frozen sections from wild-type and null mutant *Nhe2* and *Nhe3* animals were treated as described under “Experimental Procedures,” incubated overnight with the polyclonal anti-NHE2 antibody 2M5 or anti-NHE3 antibody 1314, and then treated with a fluorescein isothiocyanate-labeled secondary antibody. *Top left panel*, sections stained with NHE2-specific antibody show a strong specific staining of the apical region in the ductal lumen (arrows; the dashed line overlays the basolateral borders of the duct) and a less intense diffuse staining of the apical membranes of acinar cells. *Top right panel*, the anti-NHE2 antibody shows no specific staining of sections from *Nhe2* null mutant parotid gland. *Middle left panel*, an isolated acinus from wild-type parotid gland treated with the anti-NHE2 antibody shows specific staining of the apical region (the dashed line overlays the basolateral border of the acinus). *Middle right panel*, a Nomarski image of the same acinus shown in the *middle left panel*. *Bottom left panel*, sections from wild-type parotid gland treated with the anti-NHE3 antibody show specific staining of the apical membrane of duct cells and the adjacent sub-plasmalemmal area (arrow) but no staining of acinar cells. The dotted line corresponds to the basal membrane of the same duct. *Bottom right panel*, the anti-NHE3 antibody shows no specific staining in parotid sections prepared from *Nhe3* null mutant animals.

were performed previously (24–26), and heterozygous offspring were used to establish breeding colonies in the University of Rochester vivarium. All animals were housed in micro-isolator cages with access to laboratory chow and water *ad libitum* with a 12-hour light/dark cycle. Experiments were carried out on animals aged between 1.5 and 4 months. Body and parotid gland weights were recorded for each animal used. Homozygous *Nhe1*<sup>−/−</sup> mutants exhibited decreased rates of postnatal growth resulting in significantly lower body weights than their wild-type or heterozygous littermates, exhibited an ataxic gait, and became prone to epileptic seizures that ended in a catatonic-like state, from which the animal usually recovered (24). In our experiments, mean body weights (g) for NHE1 animals were  $30.8 \pm 2.2$  (+/+,  $n = 11$ ) and  $16.4 \pm 2.2$  (−/−,  $n = 12$ ,  $p < 0.01$  compared with +/+, Student's *t* test). The magnitude of the body weight loss (>45%) did not correlate with a comparable decrease in parotid gland weight (~7%); parotid weights (mg) were  $33.9 \pm 2.4$  (+/+,  $n = 12$ ) and  $31.5 \pm 1.9$  (−/−,  $n = 12$ ,  $p = 0.5$ ).

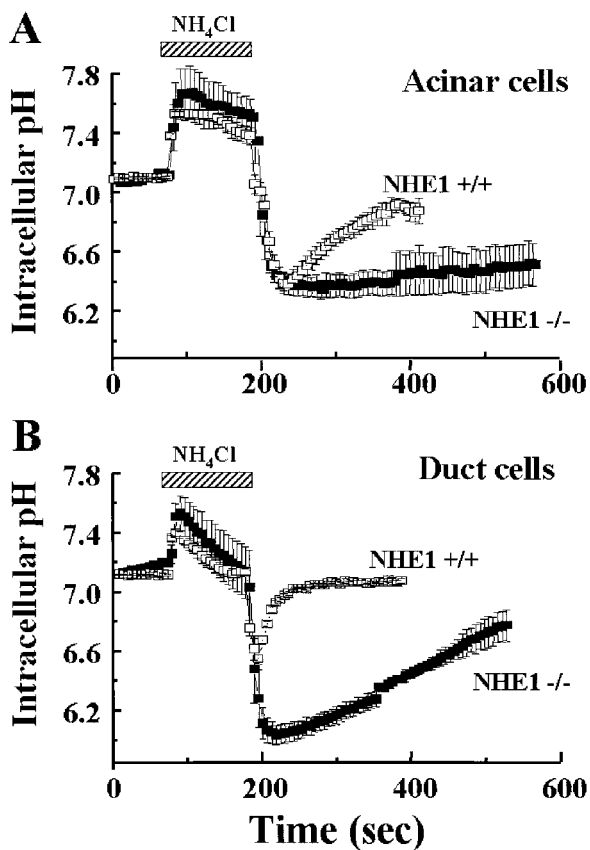


**FIG. 3. NHE1-dependent  $\text{Na}^+/\text{H}^+$  exchanger activity in acinar and duct cells isolated from mouse parotid gland.** Carboxy SNARF1-acetoxymethyl ester-loaded mouse parotid acini and ducts prepared by collagenase digestion from wild-type and *Nhe1*<sup>-/-</sup> animals (see “Experimental Procedures”) were acid-loaded by the addition and subsequent removal of 30 mM NH<sub>4</sub>Cl (during the time periods indicated by the hatched bars). *A*, acini isolated from wild-type animals (open symbols) rapidly recover from an intracellular acidification, whereas recovery is inhibited in *Nhe1*<sup>-/-</sup> mice more than 95% (filled symbols). *B*, recovery from an intracellular acid load is about 3-fold faster in wild-type duct cells (open symbols) than in acini. In *Nhe1* null mutant mice (filled symbols) recovery from intracellular acidification is reduced ~80% compared with that seen in ducts from wild-type animals. Each trace is the average response of eight or more experiments.

14). *Nhe2* and *Nhe3* mutant mice grew normally and exhibited the same appearance and behavior as wild-type animals (25, 26). *Nhe2* body weights were  $30.3 \pm 0.9$  (+/+,  $n = 30$ ) and  $29.2 \pm 1.0$  (-/-,  $n = 23$ ), and parotid weights were  $33.4 \pm 1.8$  (+/+,  $n = 20$ ) and  $32.5 \pm 2.0$  (-/-,  $n = 8$ ). *Nhe3* body weights were  $32.4 \pm 1.6$  (+/+,  $n = 26$ ) and  $31.3 \pm 1.1$  (-/-,  $n = 22$ ), and parotid weights were  $45.3 \pm 3.1$  (+/+,  $n = 14$ ) and  $41.7 \pm 2.8$  (-/-,  $n = 10$ ).

**Immunohistochemistry**—For immunolocalization experiments, Na<sup>+</sup>/H<sup>+</sup> exchanger isoform NHE1 was detected using a polyclonal antibody kindly provided by Dr. J. Noel. Specific antisera for NHE2 (antibody 2M5) and NHE3 (1314) were used as described previously (27, 28). Parotid glands from *Nhe1*<sup>-/-</sup>, *Nhe2*<sup>-/-</sup>, *Nhe3*<sup>-/-</sup> (negative control), and wild-type animals were removed and immediately placed in 4% paraformaldehyde (NHE1) or frozen in 2-methylbutane on dry ice (NHE2 and NHE3). Paraformaldehyde-treated tissue was paraffin-embedded and sectioned at 4  $\mu\text{m}$ . Frozen sections (10  $\mu\text{m}$ ) were fixed and permeabilized, and nonspecific binding sites were blocked as described previously (11). Sections were incubated overnight at 4 °C in PBS, 0.8% bovine serum albumin, 0.1% gelatin, and 0.1% Triton X-100 containing 1:500 (NHE1) or 1:200 (NHE2 and NHE3) dilutions of antibody and then treated with 1:1000 Alexa 594 fluor-conjugated goat anti-rabbit (Molecular Probes, Eugene, OR) in the above buffer (NHE1) or 1:500 fluorescein isothiocyanate-labeled secondary antibody (NHE2 and NHE3, goat anti-rabbit, Jackson ImmunoResearch Laboratory, West Grove, PA) for 1 h at room temperature. Images were recorded and analyzed using a Zeiss AxioPlan microscope or a Leica confocal microscope.

**Measurement of Parotid Gland Fluid Secretion**—To avoid contami-

nation of saliva by other body fluids (e.g. tracheal and nasal secretions), saliva was collected directly from isolated parotid gland ducts. Wild-type and null mutant animals of either sex were anesthetized with chloral hydrate, and the main excretory duct of the right and left parotid glands were isolated using a dissecting microscope. Prior to saliva collection, a tracheotomy was performed to prevent asphyxiation. Secretion was initiated by the injection of the cholinergic agonist pilocarpine HCl (10 mg/kg, intraperitoneal), and saliva was collected from each duct in a calibrated glass micropipette (Sigma) by capillary flow. The rate of fluid production was measured by marking the position of the fluid front on the micropipette wall every 5 min. Each animal was weighed prior to an experiment, and parotid glands were subsequently dissected, trimmed free of connective tissue, and weighed. For data presentation, the volume of saliva secreted ( $\mu\text{l}$ ) and the rate of parotid saliva flow in  $\mu\text{l}/\text{min}$  were normalized to 100 mg parotid gland weight. Results are expressed as mean  $\pm$  S.E. of the saliva flow from both the right and left glands from  $n$  animals measured at each time point.

Collected saliva samples were analyzed for total sodium and potassium content by atomic absorption using a Perkin-Elmer 3030 spectrophotometer. Sample osmolality was measured using a Wescor 5500 Vapor Pressure Osmometer, and chloride activity was estimated using an Orion EA 940 expandable ion analyzer.

**Northern Blot Analysis**—Total RNA was isolated from the parotid glands of mice using Trizol reagent (Life Technologies, Inc.) followed by poly(A)<sup>+</sup> mRNA selection using an Oligotex mRNA kit from Quiagen. For Northern analysis, each gland sample was pooled from three or more mice. Northern blots were prepared and hybridized as described previously (6) using <sup>32</sup>P-labeled cDNA probes for NKCC1 (rat nts 3368–3563, GenBank™ accession number AF051561), Cl<sup>-</sup>/HCO<sub>3</sub><sup>-</sup> exchanger isoform 2 (mouse nts 1300–1776, GenBank™ accession number J04036), NHE3 (rat nts 1857–2378, GenBank™ accession number M85300),  $\alpha$ -ENaC (mouse nts 931–1185, GenBank™ accession number AF112185),  $\beta$ -ENaC (mouse nts 160–380, GenBank™ accession number U16023), and  $\gamma$ -ENaC (mouse nts 1882–2184, GenBank™ accession number AF112187). A cDNA for mouse ribosomal messenger RNA L32 (mouse nts 3072–3244, GenBank™ accession number K02060) was used to normalize the expression between preparations. For dot blots, mRNA was isolated from the parotid glands of individual animals. Ten separate replicate dot blots were prepared using each mRNA sample. Each blot was hybridized with both a specific probe (as described above) then stripped and probed with L32 cDNA. Quantitation was performed by PhosphorImager analysis (Bio-Rad).

**Acinar Cell Preparation and Intracellular pH Measurements**—Parotid acini (5–20 cells) were prepared from wild-type and knockout littermates by collagenase digestion (29). In brief, glands were minced in Earle’s minimum essential medium (Biofluids, Rockville, MD) supplemented with 0.075 units/ml collagenase P, 2 mM glutamine, and 0.1% bovine serum albumin and incubated in the same medium at 37 °C for 75 min. The final acinar preparation was loaded with a pH-sensitive fluorescent indicator by incubation with 2  $\mu\text{M}$  carboxy SNARF1-acetoxymethyl ester (Molecular Probes) for 30 min in a physiological salt solution. Experiments to measure intracellular pH were carried out in physiological salt solution containing (in mM): 135 NaCl, 5.4 KCl, 1.2 CaCl<sub>2</sub>, 0.8 MgSO<sub>4</sub>, 0.33 Na<sub>2</sub>PO<sub>4</sub>, 0.4 KH<sub>2</sub>PO<sub>4</sub>, 10 glucose, and 20 Hepes (pH 7.4 with NaOH). NH<sub>4</sub>Cl-containing physiological salt solution was made by substituting 30 mM NaCl with 30 mM NH<sub>4</sub>Cl. Intracellular fluorescence was monitored in ratio mode from acini and ducts adhering to the base of a superfusion chamber mounted on an Ultima™ confocal microscope (Genomic Solutions, Ann Arbor, MI). Cells were excited at 514 nm and emitted fluorescence measured at 570 and  $\geq 630$  nm. Intracellular pH was estimated by *in situ* calibration of the excitation ratio using the high K<sup>+</sup>/nigericin protocol as described previously (30). Na<sup>+</sup>/H<sup>+</sup> exchanger activity was monitored after an NH<sub>4</sub>Cl-induced acid load (31).

**Morphological Analyses**—For light and electron microscopic studies of the parotid gland, mice were anesthetized with Ketamine/Xylazine (100 mg/10 mg, intraperitoneal) and perfused intracardially with 2.5% glutaraldehyde in 0.1 M sodium cacodylate buffer (pH 7.4). The glands were excised, immersed in fixative for an additional 3–4 h, then trimmed into small pieces, and rinsed in 0.1 M cacodylate buffer. The tissues were post-fixed in 1% osmium tetroxide/0.8% potassium ferricyanide in cacodylate buffer and then stained in block with 0.5% aqueous uranyl acetate. After dehydration in graded ethanol solutions and substitution with propylene oxide, the tissues were embedded in Polybed epoxy resin (Polysciences). For light microscopy, 1- $\mu\text{m}$  sections were stained with methylene blue-Azur II and examined in a Leitz Orthoplan microscope. Thin sections were stained with uranyl acetate

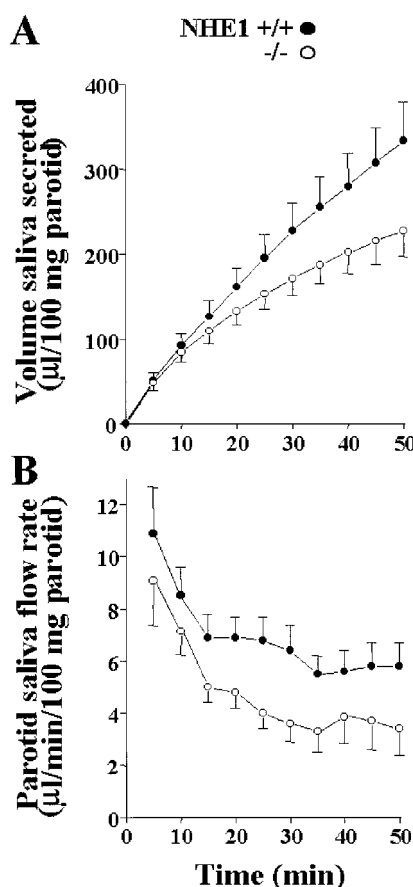


**FIG. 4. Targeted disruption of the *Nhe1* gene inhibits muscarinic-induced saliva secretion *in vivo*.** Parotid gland salivation was measured in anesthetized littermate wild-type and null mutant *Nhe1* mice as described under “Experimental Procedures.” A shows the cumulative volume of saliva secreted over time, and B displays the parotid saliva flow rate normalized to gland wet weight. A, targeted disruption of the *Nhe1* gene (open circles) significantly reduces the volume of stimulated saliva produced over a 50-min time course compared with wild-type animals (solid circles). B, deletion of NHE1 expression induces a marked reduction in the rate of saliva secretion. Data are means  $\pm$  S.E. for 12 parotid glands from 6 individual animals (+/+) and 16 glands from 8 animals (-/-).

and lead citrate and examined in a Philips CM10 transmission electron microscope.

## RESULTS

**Localization of NHE Proteins in Mouse Parotid Gland—** Previous reports have demonstrated that the distribution of the different NHE isoforms is species- and salivary gland type-specific. Thus, to better understand the precise function(s) of the various NHE isoforms expressed in mouse parotid glands we first documented their distribution by immunohistochemistry. NHE1 has been localized to the basolateral membrane of acinar and duct cells in rat parotid (10, 23) and submandibular glands (11, 12). NHE2 and NHE3 are located in the apical membranes of submandibular ducts and acini, whereas only NHE3 was detected in the ductal apical membrane of the rat parotid gland (10). The top left panel of Fig. 1 shows that NHE1 is localized to the basolateral membrane of acinar cells in wild-type mice. No labeling was detected in parotid sections from *Nhe1*<sup>-/-</sup> null mutant mice (top right panel), verifying the specificity of the antibody. Much more intense staining was seen in the ducts of parotid gland. An image of a duct in cross-section is shown in the middle left panel of Fig. 1, where the intensity of the illumination was reduced relative to that used in the top left panel to prevent overexposure. The middle

right panel of Fig. 1 is a Nomarski image of the duct shown in the middle left panel. To more clearly demonstrate the acinar localization of NHE1, parotid cells were dispersed by treatment with collagenase. Consistent with the staining observed in tissue sections (top left panel), NHE1 is expressed in the basolateral membrane of isolated acinar cells (bottom left panel). A Nomarski image of this acinus is provided in the bottom right panel of Fig. 1. These data confirm the targeting of NHE1 to the basolateral membranes of mouse parotid acinar and duct cells.

In contrast to NHE1 staining, the top left panel of Fig. 2 shows that NHE2 protein was distributed primarily to the apical membranes of duct cells (strong specific apical staining is indicated by arrows; note that the basal borders of the duct are overlaid by dashed lines). Much less intense staining of the apical membrane of acinar cells was detected; in fact, in some acini, expression of NHE2 protein was either absent or too low to be detected. The antibody used was specific because parotid sections from *Nhe2* null mutants showed an absence of staining (top right panel). Parotid glands were dispersed by treatment with collagenase to more clearly demonstrate the localization of NHE2 in acinar cells. In agreement with the staining observed in tissue sections (top left panel), NHE2 was primarily expressed in the apical region of isolated acinar cells (middle left panel; the outline of the acinus is represented by the dashed line). A Nomarski image of this acinus is provided in the middle right panel of Fig. 2. NHE3 protein was not detected in parotid acinar cells but only in the apical region of duct cells (arrow in the bottom left panel of Fig. 2; the basal border of the duct cut in cross-section is overlaid by a dashed line). No staining was detected in NHE3-deficient mice (bottom right panel of Fig. 2).

**Intracellular pH Regulation Is Severely Impaired in Acinar and Duct Cells Isolated from *Nhe1*<sup>-/-</sup> Mice—***Nhe1*, *Nhe2*, and *Nhe3* null mutant animals were used to examine the contribution of each isoform to pH regulation in parotid acinar and duct cells. The NH<sub>4</sub><sup>+</sup> pulse method was used to acid-load cells to monitor Na<sup>+</sup>/H<sup>+</sup> exchanger activity. The average intracellular pH responses to this manipulation in acinar cells isolated from wild-type (+/+, dotted line) and NHE1-deficient animals (-/-, solid line) are shown in Fig. 3A. Removal of NH<sub>4</sub>Cl led to an intracellular acidification followed by an intracellular pH recovery, and this recovery was inhibited by more than 95% in NHE1-deficient mice, whereas disruption of the *Nhe2* and *Nhe3* genes (data not shown) had little or no effect on recovery rates (see also Ref. 29). Duct cells isolated from *Nhe1*<sup>+/+</sup> animals (+/+, dotted line) also recovered their intracellular pH (Fig. 3B) but at an initial rate nearly 3-fold faster than that of acinar cells. The more robust Na<sup>+</sup>/H<sup>+</sup> exchanger activity in duct cells likely reflects the higher expression of Na<sup>+</sup>/H<sup>+</sup> exchangers in this cell type (see Figs. 1 and 2). The magnitude of the inhibition of pH recovery caused by disruption of the *Nhe1* gene was less dramatic in duct cells (~80%, -/-, solid line). This result correlates with the abundance of NHE2 and NHE3 in ducts (see Fig. 2). Moreover, the residual pH recovery in duct cells from NHE1-deficient mice was about an order of magnitude more resistant to the amiloride derivative ethylisopropyl amiloride than ducts from wild-type mice (data not shown), in agreement with immunological staining suggesting that NHE3 is strongly expressed in this cell type. These results confirm that NHE1 is the major regulator of intracellular pH in mouse parotid acinar cells and also demonstrate that NHE1 contributes to pH regulation in duct cells, albeit less significantly.

***NHE1* and *NHE2* Regulate Pilocarpine-induced Salivation in Vivo—** Earlier studies using the Na<sup>+</sup>/H<sup>+</sup> exchange inhibitor amiloride and its analogs suggested that Na<sup>+</sup>/H<sup>+</sup> exchangers may be involved in salivation. Localization of NHE1 and NHE2 (Figs. 1 and 2, respectively) to acinar cells suggests that one or

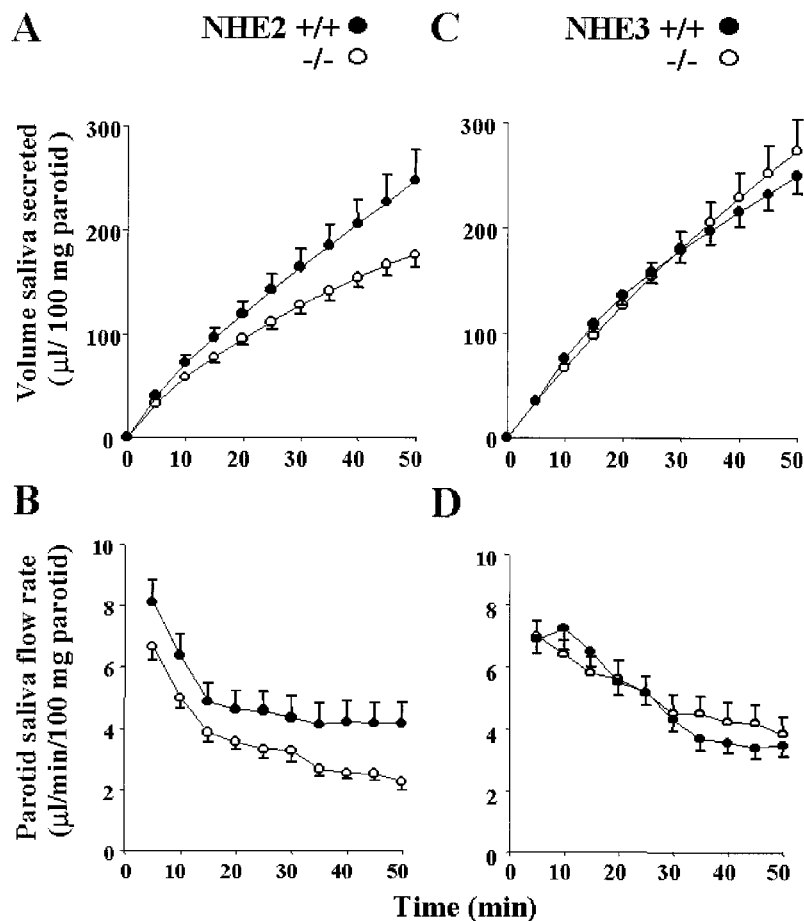


**FIG. 5. Effects of targeted disruption of the *Nhe2* and *Nhe3* genes on muscarinic-induced saliva secretion *in vivo*.** Parotid gland salivation was measured in anesthetized littermate wild-type and null mutant *Nhe2* and *Nhe3* mice as described in the Fig. 4 legend. *A*, targeted disruption of the *Nhe2* gene (open circles) significantly reduces the volume of stimulated saliva produced over a 50-min time course compared with *+/+* animals (solid circles). *B*, deletion of NHE2 expression induces a marked reduction in the rate of saliva secretion. Data are means  $\pm$  S.E. for 23 glands from 12 animals (*+/+*) and 28 glands from 14 animals (*-/-*). *C*, targeted disruption of the *Nhe3* gene (open circles) does not significantly alter the volume of stimulated saliva produced over a 50-min time course compared with *+/+* animals (solid circles). *D*, deletion of NHE3 expression has no effect on the rate of saliva secretion. Data are means  $\pm$  S.E. for 22 parotid glands from 11 individual animals (*+/+*) and 22 glands from 12 animals (*-/-*).

both of these isoforms might contribute to secretion. To directly test the role of each NHE isoform, parotid saliva was collected from *Nhe1*, *Nhe2*, or *Nhe3* wild-type and null mutant mice over a 50-min time period. Fig. 4A shows that targeted disruption of *Nhe1* (open circles) reduced the total volume of pilocarpine-stimulated saliva secreted during the 50-min collection period by 34% compared with wild-type animals (solid circles). The magnitude of the decrease in flow rate increased over time. The flow rate was reduced by 16% during the first 5 min and reached 42% inhibition at the end of the 50-min collection period (Fig. 4B).

Likewise, disruption of NHE2 expression reduced the total volume of saliva secreted by 29% (Fig. 5A), and the effect on the flow rate increased during prolonged stimulation from 18% during the first 5 min to 46% inhibition at 50 min (Fig. 5B). In contrast, normal salivation was observed in NHE3-deficient mice (Fig. 5, C and D). For all genotypes, note the high initial flow rate seen at the commencement of secretion, which declines to a lower relatively constant rate thereafter. The secretion kinetics and flow rates are similar to those reported previously (6, 32).

**Targeted Disruptions of *Nhe2* and *Nhe3* Genes Fail to Inhibit Na<sup>+</sup> Absorption by Duct Cells**—The initial step in the formation of saliva is the secretion of a plasma-like NaCl-rich fluid from acinar cells. Subsequently, duct cells reabsorb much of the secreted NaCl to produce a hypotonic NaCl-poor saliva. Na<sup>+</sup>/H<sup>+</sup> exchangers play a major role in NaCl absorption in other epithelia, although it is unknown whether they serve a similar function in salivary glands. To examine this possibility, parotid saliva was collected from *Nhe1*, *Nhe2*, or *Nhe3* wild-type and null mutant mice, and the sodium and potassium content, Cl<sup>-</sup> activity, and osmolality were determined. Table I shows that the ion content and the osmolality of saliva collected

from NHE2- and NHE3-deficient mice were comparable with secretions from littermate wild-type mice, suggesting that these Na<sup>+</sup>/H<sup>+</sup> exchangers do not play a major role in NaCl reabsorption in this tissue. In contrast, the osmolality and sodium, potassium, and chloride content increased significantly in saliva from *Nhe1*<sup>-/-</sup> mice.

**Morphology of the Parotid Gland in NHE1-, NHE2-, and NHE3-deficient Mice**—NHE1 and NHE2 are expressed in the basolateral and apical membranes, respectively, of acinar cells, and targeted disruption of the *Nhe1* and *Nhe2* genes inhibited secretion (Figs. 4 and 5). By examining the morphology of affected organs, it is sometimes possible to visualize changes induced by gene disruption that might compensate for the loss of function (24–26). To test the hypothesis that morphological changes reflect activation of compensatory mechanisms in the parotid glands of NHE-deficient mice, parotid glands were examined by light and electron microscopy. Fig. 6 shows that the size and appearance of parotid acinar cells were comparable in wild-type (A), NHE1-deficient (B), NHE2-deficient (C), and NHE3-deficient (D) mice. Thus, no obvious morphological changes were apparent that could explain the reduced production of saliva by mice lacking NHE1 or NHE2. Moreover, the size of the acinar and duct cells and the ratio of acinar to ductal elements in the glands appeared comparable, although detailed morphometric analyses to confirm these observations were not performed.

NHE1 is highly expressed in the basolateral membranes of duct cells (Fig. 1). No differences in morphology between *Nhe1*<sup>+/+</sup> (A) and *Nhe1*<sup>-/-</sup> (B) mice were observed in electron micrographs of duct cells (Fig. 7). The apical cell surface and junctional complexes, extent of basolateral membrane infolding, and the size and number of mitochondria in the striated duct cells appeared similar in the knockout and wild-type mice.

TABLE I

Targeted disruption of murine *Nhe1*, *Nhe2*, and *Nhe3* genes: effects on osmolality, sodium content, potassium content, and chloride activity of pilocarpine-stimulated saliva

Stimulated saliva was collected for 50 min from mouse parotid glands, and the osmolality and ionic composition were determined for the 10–50-min collection period (saliva collected during the first 10 min gave comparable results). Osmolality was measured using a vapor pressure osmometer. Sodium and potassium content were analyzed by atomic absorption (see “Experimental Procedures”). Chloride activity was estimated using an Orion EA 940 expandable ionanalyzer.

	NHE1		NHE2		NHE3	
	+/+	-/-	+/+	-/-	+/+	-/-
Osmolality (mmol/kg)	189.6 ± 14.6	253.0 ± 12.8 <sup>a</sup>	178.1 ± 6.4	173.3 ± 4.9	168.7 ± 6.1	175.6 ± 6.2
[Sodium] (mM)	78.0 ± 10.2	98.8 ± 8.9 <sup>b</sup>	75.7 ± 4.7	63.9 ± 3.6*	69.4 ± 4.9	71.8 ± 4.2
[Potassium] (mM)	14.1 ± 0.9	19.0 ± 1.7 <sup>b</sup>	20.4 ± 0.8	22.0 ± 0.9	19.1 ± 0.9	16.6 ± 0.7 <sup>b</sup>
Cl <sup>-</sup> (mM)	94.1 ± 13.0	155.6 ± 13.7 <sup>a</sup>	75.6 ± 6.2	72.1 ± 9.2	94.7 ± 8.5	86.3 ± 6.4

Significantly different from +/+: <sup>a</sup> p < 0.0003 (Student's *t* test), <sup>b</sup> p < 0.05. n ≥ 10.

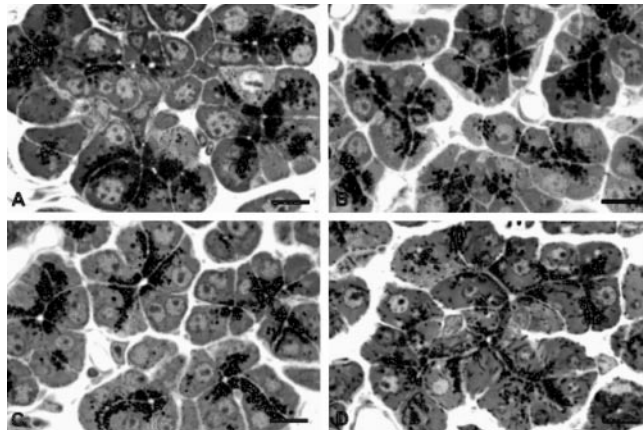


FIG. 6. Morphology of parotid gland acinar cells in wild-type, *Nhe1*<sup>-/-</sup>, *Nhe2*<sup>-/-</sup>, and *Nhe3*<sup>-/-</sup> mice. Light micrographs of wild-type (A), *Nhe1*<sup>-/-</sup> (B), *Nhe2*<sup>-/-</sup> (C), and *Nhe3*<sup>-/-</sup> (D) parotid glands. One-μm sections were stained with methylene blue-Azur II and examined in a Leitz Orthoplan microscope. Acinar cell structures in A–D appear similar. Scale bars, 10 μm.

**Compensatory Mechanisms in NHE1, -2, and -3 Null Mutant Mice**—Given the important role of NHE1 in the regulation of both intracellular pH (29, 33) and the secretion of saliva (Fig. 4) and recent results indicating that the loss of NHE3 can be partially compensated for by altering the expression of other ion transport proteins in the large intestine (26) and kidney (34), we assessed whether disruption of the *Nhe* genes perturbed the expression of ion transport proteins involved in saliva secretion from the parotid gland. The level of the mRNA coding for six different proteins was determined: α-ENaC, β-ENaC, γ-ENaC, NKCC1, Cl<sup>-</sup>/HCO<sub>3</sub><sup>-</sup> exchanger isoform 2, and NHE3 (Table II). First, mRNA was pooled from three *Nhe1*<sup>+/+</sup>, -2<sup>+/+</sup>, or -3<sup>+/+</sup> or three *Nhe1*<sup>-/-</sup>, -2<sup>-/-</sup>, or -3<sup>-/-</sup> mice and then separated, and transcript levels were determined via Northern analysis. Second, six replicate membranes were dot-blotted using mRNA prepared from individual mice (three *Nhe1*<sup>+/+</sup>, -2<sup>+/+</sup>, or -3<sup>+/+</sup> and three *Nhe1*<sup>-/-</sup>, -2<sup>-/-</sup>, or -3<sup>-/-</sup>) and then probed for each of the six transcripts to assess variability between mice. In all cases, a PhosphorImager was used to quantitate the labeled transcripts, and the specific band(s) of interest on the Northern blots contributed greater than 80% of the signal (data not shown). The data obtained using dot-blot analyses generally mirrored those obtained through Northern analysis (Table II). The most notable change in expression occurred in the parotid glands of *Nhe1*<sup>-/-</sup> mice, in which the level of NKCC1 mRNA was increased nearly 3-fold over wild type. The upper left panel of Fig. 8 demonstrates this increase. In contrast, only subtle changes in NKCC1 mRNA expression were noted in *Nhe2*<sup>-/-</sup> and *Nhe3*<sup>-/-</sup> mice (Fig. 8). In addition, the level of NHE3 mRNA increased by almost 2-fold in the parotid glands of *Nhe2*<sup>-/-</sup> mice relative to wild type (Table II

and Fig. 8, upper right panel). All of the ENaC subunits (α, β, and γ) were slightly elevated in the parotids of the *Nhe2*<sup>-/-</sup> and *Nhe3*<sup>-/-</sup> mice, as well (Table II).

## DISCUSSION

Several lines of evidence suggest that Na<sup>+</sup>/H<sup>+</sup> exchange plays an important role in both fluid secretion and Na<sup>+</sup> absorption by salivary glands (7, 8, 18–21, 35, 36), although the specific NHE isoforms involved are unknown. Thus, the focus of the current study was to directly test two hypotheses: first, basolateral NHE1 plays an important role in acinar cell fluid secretion, and second, the NHE2 and NHE3 located in the apical membranes of duct cells modulate the final composition of saliva by reabsorbing Na<sup>+</sup>. To examine the functions of these exchangers, we investigated the *in vivo* consequences of disrupting the expression of individual NHE isoforms on the regulation of salivary gland secretion. The functional effects of mutating the murine *Nhe1* (24, 37), *Nhe2* (25), and *Nhe3* (26) genes have been described in other tissues, and these studies have uncovered several unexpected consequences of knocking out individual NHE isoforms. For example, the loss of NHE1 expression failed to produce functional deficits in organs such as the kidney and intestine but instead resulted in an epileptic and ataxic phenotype (24, 37). NHE1 had not been predicted previously to play such a role in the central nervous system. Moreover, NHE2 seems not to be critically involved in NaCl reabsorption as expected previously for the kidney and intestinal tract but instead is required for maintaining the long-term survival of gastric parietal cells (25). Consequently, previous studies to identify transport mechanisms that unavoidably relied on inhibitors with limited selectivity or ion substitution protocols were clearly inadequate to verify the specific functions of individual NHE isoforms.

NHE1 was localized to the basolateral membrane of mouse parotid acinar and duct cells in the present study, consistent with the predicted location of NHE1 in salivary glands (10–12, 23). Previous *in vitro* studies in mouse parotid acinar cells directly established that NHE1 is the Na<sup>+</sup>/H<sup>+</sup> exchanger isoform up-regulated by muscarinic receptor stimulation (29) and thus is the exchanger most likely to have a major role in modulating the rate of secretion (23, 35, 36). The present *in vivo* functional studies revealed that the knockout of *Nhe1* gene expression inhibited pilocarpine-induced salivary flow, with the magnitude of the inhibition increasing during sustained stimulation.

NHE1 almost certainly regulates secretion by promoting an increase in the intracellular pH. This alkalinization facilitates secretion by at least two mechanisms. The first of these is apical HCO<sub>3</sub><sup>-</sup> secretion, which depends on the activity of carbonic anhydrase and Na<sup>+</sup>/H<sup>+</sup> exchange. The second secretion mechanism relies on transepithelial Cl<sup>-</sup> movement driven by paired basolateral Na<sup>+</sup>/H<sup>+</sup> and Cl<sup>-</sup>/HCO<sub>3</sub><sup>-</sup> exchangers (see Ref. 5). It is also interesting to note that the rate of secretion during

**FIG. 7. Ultrastructure of parotid gland duct cells in wild-type and *Nhe1*<sup>-/-</sup> mice.** Electron micrographs of wild-type (A) and *Nhe1*<sup>-/-</sup> (B) parotid gland striated ducts. Thin sections were stained with uranyl acetate and lead citrate and examined in a Philips CM10 transmission electron microscope. Ductal cell structure in wild-type and null mutant *Nhe1*<sup>-/-</sup> glands appears similar. Basal infoldings are well developed, and mitochondria are numerous in the cells of both wild-type and null mutant *Nhe1*<sup>-/-</sup> glands. Scale bars, 1  $\mu$ m.

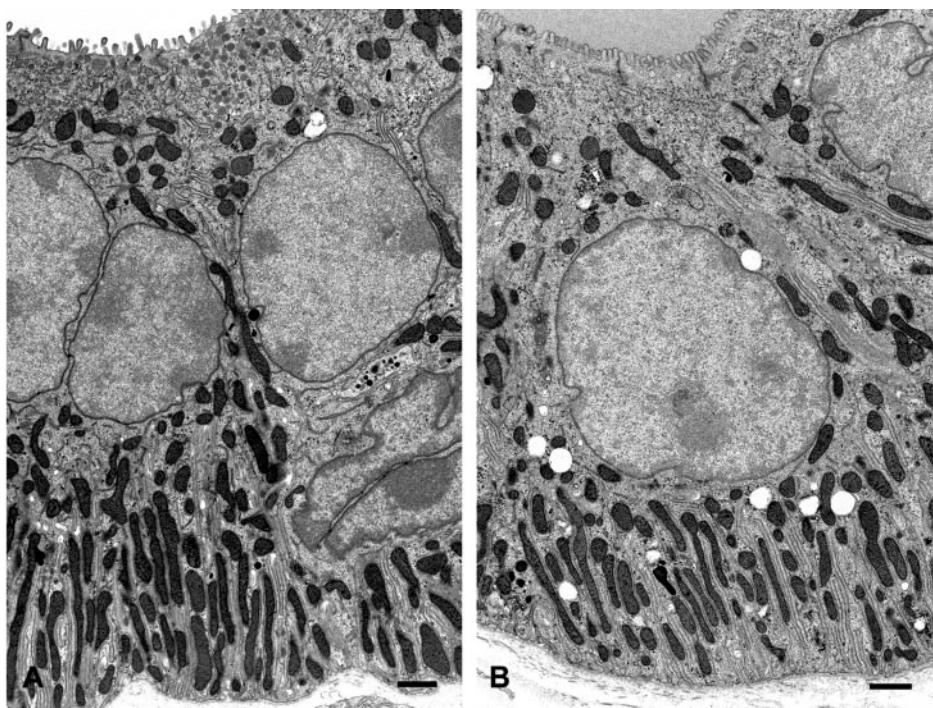


**TABLE II**  
*Northern and dot-blot analysis of ion transport protein mRNA: compensatory mechanisms in Nhe null mutant mice*

The level of mRNA expression for each of six ion transport proteins isolated from the parotid glands of *Nhe1*<sup>-/-</sup>, *Nhe2*<sup>-/-</sup>, and *Nhe3*<sup>-/-</sup> mice is shown relative to expression in the parotid glands of wild-type littermates (set at 100%). Experiments were done using pooled parotid glands ( $n = 3$ ) for Northern analysis and individual parotid glands ( $n = 3$ ) for dot-blot analysis. All experiments were normalized to L32 ribosomal protein mRNA. The values indicated in bold represent the most significant and reproducible changes observed.

mRNA	Northern	Mouse 1	Mouse 2	Mouse 3
<i>Nhe1</i> <sup>-/-</sup>	$\alpha$ -ENaC	112	78	101
<i>Nhe2</i> <sup>-/-</sup>	$\alpha$ -ENaC	104	106	89
<i>Nhe3</i> <sup>-/-</sup>	$\alpha$ -ENaC	116	116	118
<i>Nhe1</i> <sup>-/-</sup>	$\beta$ -ENaC	96	93	99
<i>Nhe2</i> <sup>-/-</sup>	$\beta$ -ENaC	127	109	116
<i>Nhe3</i> <sup>-/-</sup>	$\beta$ -ENaC	124	145	119
<i>Nhe1</i> <sup>-/-</sup>	$\gamma$ -ENaC	107	108	98
<i>Nhe2</i> <sup>-/-</sup>	$\gamma$ -ENaC	114	101	116
<i>Nhe3</i> <sup>-/-</sup>	$\gamma$ -ENaC	133	143	119
<i>Nhe1</i> <sup>-/-</sup>	<b>NKCC1</b>	<b>258</b>	<b>290</b>	<b>350</b>
<i>Nhe2</i> <sup>-/-</sup>	NKCC1	91	105	85
<i>Nhe3</i> <sup>-/-</sup>	NKCC1	130	110	119
<i>Nhe1</i> <sup>-/-</sup>	AE2	96	94	79
<i>Nhe2</i> <sup>-/-</sup>	AE2	110	107	98
<i>Nhe3</i> <sup>-/-</sup>	AE2	122	110	97
<i>Nhe1</i> <sup>-/-</sup>	NHE3	107	106	98
<i>Nhe2</i> <sup>-/-</sup>	<b>NHE3</b>	<b>194</b>	<b>159</b>	<b>172</b>
<i>Nhe3</i> <sup>-/-</sup>	NHE3	<10%	<10%	<10%

the initial 10 min of stimulation was reduced only by ~17% in *Nhe1*<sup>-/-</sup> mice, but the reduction in the rate of secretion was nearly 35% for the next 10-min interval. This subtle effect on the initial phase of secretion, but greater effect after 10 min of stimulation in NHE1-deficient mice, correlates with the time dependence (5–10 min of stimulation) necessary to produce an intracellular alkalinization in acinar cells (8) and the covalent activation of the exchanger (38). It is also worth noting that NKCC1 is the major chloride influx pathway during the early stages of salivation; however, the contribution of  $\text{Na}^+/\text{K}^+/2\text{Cl}^-$  cotransporter activity decreases during prolonged stimulation (6). Thus, the residual parotid saliva produced by *Nhe1*<sup>-/-</sup> mice during the first 10 min of stimulation (83% of that measured in wild-type mice) is equivalent to the inhibition of secretion (nearly 80%) observed during this time period in NKCC1-deficient mice (6). Moreover, after 50 min of stimulation, the 42% decrease in flow rate in *Nhe1*<sup>-/-</sup> mice was comparable with the residual saliva (45%) secreted by NKCC1-deficient mice (6).

Together, these data clearly demonstrate that both NHE1 and NKCC1 are involved in salivary gland secretion and that their relative contributions to this process vary during prolonged stimulation.

NHE1 activity presumably modulates the activity of other ion transport pathways involved in the fluid secretion process. Indeed, patch clamp studies have demonstrated previously that low cytosolic pH (pH 6.8) inhibits and higher values (pH 7.3, 7.8) enhance the activity of apical  $\text{Ca}^{2+}$ -dependent  $\text{Cl}^-$  currents in rat parotid (39) and lacrimal (40) acinar cells. Clearly then, by maintaining the intracellular pH at a higher value, NHE1 provides a greater driving force for  $\text{Cl}^-$  and  $\text{HCO}_3^-$  exit across the apical membrane via the apical anion channel(s) and, by functional coupling, enhances  $\text{Cl}^-$  entry across the basolateral membrane via the  $\text{Cl}^-/\text{HCO}_3^-$  exchanger. As a specific consequence of NHE1 loss of function, mRNA expression of the  $\text{Na}^+/\text{K}^+/2\text{Cl}^-$  cotransporter NKCC1 was increased. The mechanism for increasing the expression of the

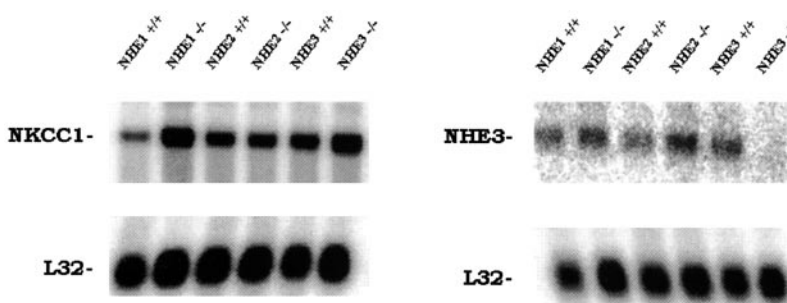


**FIG. 8. Effects of targeted disruption of the *Nhe* genes on NKCC1 and NHE3 mRNA expression in parotid glands.** Poly(A)<sup>+</sup>-selected mRNA was isolated from the parotid glands of wild-type and NHE1-deficient (left columns), NHE2-deficient (middle columns) and NHE3-deficient (right columns) mice, and 2.5  $\mu$ g of mRNA was loaded per lane as described under “Experimental Procedures.” Upper left row, the blot was probed with a rat NKCC1 cDNA. Upper right row, the blot was hybridized with a mouse NHE3 probe. Lower rows, the blots were stripped and hybridized with a mouse ribosomal mRNA L32 probe.

major Cl<sup>-</sup> uptake pathway in acinar cells is unclear. Regardless, by increasing Cl<sup>-</sup> uptake via NKCC1, a partial compensation for decreased salivary flow may have occurred in *Nhe1*<sup>-/-</sup> animals.

The subcellular localization of NHE2 and NHE3 to the apical membrane in mouse parotid duct cells (Fig. 2) is generally consistent with previous reports for rat parotid gland (10) and the proposed role of these isoforms in salt reabsorption in epithelial cells (41, 42). However, the presence of NHE2 in mouse parotid acinar cells suggests a species-specific difference compared with rat, where immunohistochemistry using the same antibody used in this study combined with semi-quantitative reverse transcription-polymerase chain reaction failed to detect either NHE2 protein or NHE2 transcript in rat parotid (10) or rat submandibular (11) glands. Surprisingly, disruption of the *Nhe2* gene blunted *in vivo* stimulated saliva by mouse parotid acinar cells (salivary gland duct cells do not secrete fluid; for a discussion see Ref. 5), which is functional confirmation consistent with the acinar localization of the NHE2 isoform.

So what then is the function of the apical NHE2 in salivary acinar cells? In other epithelia this isoform is inhibited when the intracellular [Ca<sup>2+</sup>] increases (43). Thus, muscarinic stimulation might be expected also to inhibit NHE2 activity in parotid acinar cells. However, NHE2 is uniquely sensitive to extracellular pH, with extracellular protons inhibiting activity ( $pK_a$  for extracellular H<sup>+</sup> ~ 7.9; see Ref. 44). Because parotid acini secrete HCO<sub>3</sub><sup>-</sup> during stimulated fluid secretion, one would expect the extracellular pH of the acinar lumen (a very small compartment) to be alkaline, thereby increasing NHE2 activity. Operating in this mode it is possible that the function of NHE2 is to provide a secondary mechanism (in addition to NHE1) for regulating the intracellular pH of the apical membrane microdomain, thus providing additional “fine-tuning” by which to regulate the activity of the Ca<sup>2+</sup>-activated Cl<sup>-</sup> channel during muscarinic receptor-induced fluid secretion. This is but one possible explanation for the observation that salivation was decreased in pilocarpine-stimulated *Nhe2*<sup>-/-</sup> mice (Fig. 5), and further studies are clearly required to directly test this possibility.

NHE2 and NHE3 are thought to mediate Na<sup>+</sup> absorption in tissues such as the kidney and intestine (see Refs. 41 and 42). Therefore, it was surprising to find that saliva from NHE2- and NHE3-deficient mice had equivalent NaCl content and osmolality to that collected from wild-type littermates (Table I). The lack of functional consequences on the final composition of saliva after either *Nhe2* or *Nhe3* gene disruptions clearly demonstrates that these Na<sup>+</sup>/H<sup>+</sup> exchangers are not the main pathway for Na<sup>+</sup> absorption by parotid duct cells. It is interesting to note, however, that the transcripts for the  $\alpha$ ,  $\beta$ , and  $\gamma$

subunits of ENaC were slightly increased in the *Nhe2*<sup>-/-</sup> and *Nhe3*<sup>-/-</sup> mice (Table II). ENaC may serve as the primary conduit for Na<sup>+</sup> reabsorption in parotid duct cells, whereas NHE2 and NHE3 play a smaller role. If this were the case, then the loss of NHE2 and NHE3 would be easily compensated for by the increased ENaC levels.

It is important to note that the recovery of NaCl by the duct cells is a flow rate-dependent process (5). Thus, the *Nhe1* null mutant animals would be expected to have decreased levels of sodium, potassium, and chloride and decreased osmolality given their reduced rates of secretion. That the opposite is in fact true speaks strongly for the role NHE1 must play in duct cell function. One contributing factor may be compromised intracellular pH regulation in duct cells, consequently inhibiting the NaCl absorption process indirectly by altering the activity of key transporters or signaling pathways. Indeed, duct cells isolated from *Nhe1*<sup>-/-</sup> mice displayed a dramatic reduction in the rate of intracellular pH recovery from an acid challenge (~80%). Alternatively, the loss of cross-talk between the basolateral NHE1 and apical membrane Na<sup>+</sup>/H<sup>+</sup> exchanger activity might explain the decreased ability of duct cells to absorb NaCl. This possibility is consistent with the functional coupling observed between apical and basolateral Na<sup>+</sup>/H<sup>+</sup> exchangers in the medullary thick ascending limb (45).

In conclusion, *Nhe1*, *Nhe2*, and *Nhe3* knockout mice provide excellent models to directly examine the functions of these Na<sup>+</sup>/H<sup>+</sup> exchangers in salivation. The present studies tested the hypothesis that basolateral NHE1 is a major regulator of fluid secretion *in vivo*. Our results are consistent with this hypothesis, because we observed a significant decrease in saliva secretion. NHE1 likely drives salivation by maintaining the sustained flux of chloride and bicarbonate ions across acinar cells by buffering “global” intracellular pH changes (29, 33). Unexpectedly, parotid secretion decreased in the NHE2 knockout mice as well, although the mechanism involved is unclear. In addition, we predicted that NHE2 and NHE3 play an important role in absorption across the apical membranes of parotid ducts, thereby modulating the ionic composition of saliva. Surprisingly, our results negate this possibility, because we observed no significant changes in the composition of saliva in the NHE2 and NHE3 knockout mice. Finally, the observation that exchanger loss of function induces the expression of related ion transport proteins suggests that by examining compensatory changes, it may be possible to better understand the functionally coupled processes that underlie salivation.

**Acknowledgments—**We thank Dr. W. Scott for providing the NHE1 knockout mice used to establish a breeding colony in Rochester. We also thank Drs. A. Menon and C. Krane for providing the mouse lung ENaC polymerase chain reaction products used as probes in Northern analysis and Dr. John Olschowka for the use of his microscope. Specific

antisera for NHE1, NHE2 (antibody 2M5), and NHE3 (1314) were provided kindly by Dr. J. Noel, Dr. C. Bookstein, and Dr. O. Moe, respectively.

## REFERENCES

- Martinez, J. R., Holzgreve, H., and Frick, A. (1966) *Pflugers Arch. Gesamte Physiol. Menschen Tiere* **290**, 124–133
- Thayesen, J. H., Thorn, N. A., and Schwartz, I. L. (1954) *Am. J. Physiol.* **178**, 155–159
- Young, J. A., and Schogel, E. (1966) *Pflugers Arch. Gesamte Physiol. Menschen Tiere* **291**, 85–98
- Melvin, J. E. (1999) *Crit. Rev. Oral Biol. Med.* **10**, 199–209
- Cook, D. I., Van Lennep, E. W., Roberts, M. L., and Young, J. A. (1994) in *Physiology of the Gastrointestinal Tract* (Johnson, L. R., ed) 3rd Ed., pp. 1061–1117, Raven Press, Ltd., New York
- Evans, R. L., Park, K., Turner, R. J., Watson, G. E., Nguyen, H. V., Dennett, M. R., Hand, A. R., Flagella, M., Shull, G. E., and Melvin, J. E. (2000) *J. Biol. Chem.* **275**, 26720–26726
- Lau, K. R., Elliott, A. C., and Brown, P. D. (1989) *Am. J. Physiol.* **256**, C288–C295
- Melvin, J. E., Moran, A., and Turner, R. J. (1988) *J. Biol. Chem.* **263**, 19564–19569
- Soltoff, S. P., McMillian, M. K., Cantley, L. C., Cragoe, E. J., Jr., and Talamo, B. R. (1989) *J. Gen. Physiol.* **93**, 285–319
- Park, K., Olschowka, J. A., Richardson, L. A., Bookstein, C., Chang, E. B., and Melvin, J. E. (1999) *Am. J. Physiol.* **276**, G470–G478
- Lee, M. G., Schultheis, P. J., Yan, M., Shull, G. E., Bookstein, C., Chang, E., Tse, M., Donowitz, M., Park, K., and Mualem, S. (1998) *J. Physiol. (Lond.)* **513**, 341–357
- He, X., Tse, C. M., Donowitz, M., Alper, S. L., Gabriel, S. E., and Baum, B. J. (1997) *Pflugers Arch. Eur. J. Physiol.* **433**, 260–268
- Couillon, L., and Pouyssegur, J. (2000) *J. Biol. Chem.* **275**, 1–4
- Orlowski, J., and Grinstein, S. (1997) *J. Biol. Chem.* **272**, 22373–22376
- Dinudom, A., Young, J. A., and Cook, D. I. (1993) *Pflugers Arch. Eur. J. Physiol.* **423**, 164–166
- Ishikawa, T., Marunaka, Y., and Rotin, D. (1998) *J. Gen. Physiol.* **111**, 825–846
- Garty, H., and Palmer, L. G. (1997) *Physiol. Rev.* **77**, 359–396
- Dissing, S., and Nauntofte, B. (1990) *Am. J. Physiol.* **259**, G1044–G1055
- Lau, K. R., Howorth, A. J., and Case, R. M. (1990) *J. Physiol. (Lond.)* **425**, 407–427
- Martinez, J. R., and Cassity, N. (1985) *Arch. Oral Biol.* **30**, 797–803
- Pirani, D., Evans, L. A., Cook, D. I., and Young, J. A. (1987) *Pflugers Arch. Eur. J. Physiol.* **408**, 178–184
- Robertson, M. A., and Foskett, J. K. (1994) *Am. J. Physiol.* **267**, C146–C156
- Robertson, M. A., Woodside, M., Foskett, J. K., Orlowski, J., and Grinstein, S. (1997) *J. Biol. Chem.* **272**, 287–294
- Bell, S. M., Schreiner, C. M., Schultheis, P. J., Miller, M. L., Evans, R. L., Vorhees, C. V., Shull, G. E., and Scott, W. J. (1999) *Am. J. Physiol.* **276**, C788–C795
- Schultheis, P. J., Clarke, L. L., Meneton, P., Harline, M., Boivin, G. P., Stemmermann, G., Duffy, J. J., Doetschman, T., Miller, M. L., and Shull, G. E. (1998) *J. Clin. Invest.* **101**, 1243–1253
- Schultheis, P. J., Clarke, L. L., Meneton, P., Miller, M. L., Soleimani, M., Gavens, L. R., Riddle, T. M., Duffy, J. J., Doetschman, T., Wang, T., Giebisch, G., Aronson, P. S., Lorenz, J. N., and Shull, G. E. (1998) *Nat. Genet.* **19**, 282–285
- Bookstein, C., Xie, Y., Rabenau, K., Musch, M. W., McSwine, R. L., Rao, M. C., and Chang, E. B. (1997) *Am. J. Physiol.* **273**, C1496–C1505
- Amemiya, M., Loffing, J., Lotscher, M., Kaissling, B., Alpern, R. J., and Moe, O. W. (1995) *Kidney Int.* **48**, 1206–1215
- Evans, R. L., Bell, S. M., Schultheis, P. J., Shull, G. E., and Melvin, J. E. (1999) *J. Biol. Chem.* **274**, 29025–29030
- Thomas, J. A., Buchsbaum, R. N., Zimniak, A., and Racker, E. (1979) *Biochemistry* **18**, 2210–2218
- Roos, A., and Boron, W. F. (1981) *Physiol. Rev.* **61**, 296–434
- Marmary, Y., Fox, P. C., and Baum, B. J. (1987) *Comp. Biochem. Physiol. A* **88**, 307–310
- Nguyen, H. V., Shull, G. E., and Melvin, J. E. (2000) *J. Physiol. (Lond.)* **523**, 139–146
- Brooks, H. L., Sorenson, A. M., Terris, J., Schultheis, P. J., Lorenz, J. N., Shull, G. E., and Knepper, M. A. (2001) *J. Physiol. (Lond.)* **530**, 359–366
- Okada, M., Saito, Y., Sawada, E., and Nishiyama, A. (1991) *Pflugers Arch. Eur. J. Physiol.* **419**, 338–348
- Seo, J. T., Larcombe-McDouall, J. B., Case, R. M., and Steward, M. C. (1995) *J. Physiol. (Lond.)* **487**, 185–195
- Cox, G. A., Lutz, C. M., Yang, C. L., Biemesderfer, D., Bronson, R. T., Fu, A., Aronson, P. S., Noebels, J. L., and Frankel, W. N. (1997) *Cell* **91**, 139–148
- Manganelli, M., and Turner, R. J. (1989) *J. Membr. Biol.* **111**, 191–198
- Arreola, J., Melvin, J. E., and Begenisich, T. (1995) *J. Membr. Biol.* **147**, 95–104
- Park, K., and Brown, P. D. (1995) *Am. J. Physiol.* **268**, C647–C650
- Wakabayashi, S., Shigekawa, M., and Pouyssegur, J. (1997) *Physiol. Rev.* **77**, 51–74
- Yun, C. H., Tse, C. M., Nath, S. K., Levine, S. A., Brant, S. R., and Donowitz, M. (1995) *Am. J. Physiol.* **269**, G1–G11
- McSwine, R. L., Musch, M. W., Bookstein, C., Xie, Y., Rao, M., and Chang, E. B. (1998) *Am. J. Physiol.* **275**, C693–C701
- Yu, F. H., Shull, G. E., and Orlowski, J. (1993) *J. Biol. Chem.* **268**, 25536–25541
- Good, D. W., George T., and Watts, B. A., III (1995) *Proc. Natl. Acad. Sci. U. S. A.* **92**, 12525–12529